

Journal of Natural Fibers

ISSN: (Print) (Online) Journal homepage: https://www.tandfonline.com/loi/wjnf20

Enhanced Sedimentation Stability of Carbonyl Iron Powders with Hydrophilic Siloxane Polymer Coatings in Ethanol

Heebo Ha, Russ Thompson & Byungil Hwang

To cite this article: Heebo Ha, Russ Thompson & Byungil Hwang (2023) Enhanced Sedimentation Stability of Carbonyl Iron Powders with Hydrophilic Siloxane Polymer Coatings in Ethanol, Journal of Natural Fibers, 20:1, 2166648, DOI: 10.1080/15440478.2023.2166648

To link to this article: https://doi.org/10.1080/15440478.2023.2166648

© 2023 The Author(s). Published with license by Taylor & Francis Group, LLC.

View supplementary material

Published online: 30 Jan 2023.

Submit your article to this journal

Article views: 146

View related articles

View Crossmark data

Full Terms & Conditions of access and use can be found at https://www.tandfonline.com/action/journalInformation?journalCode=wjnf20

JOURNAL OF NATURAL FIBERS
2023, VOL. 20, NO. 1, 2166648
https://doi.org/10.1080/15440478.2023.2166648

Taylor & Francis
Taylor & Francis Group

OPEN ACCESS Check for updates

Enhanced Sedimentation Stability of Carbonyl Iron Powders with Hydrophilic Siloxane Polymer Coatings in Ethanol

Heebo Ha[a], Russ Thompson[b], and Byungil Hwang[a]

[a]School of Integrative Engineering, Chung-Ang University, Seoul, Republic of Korea; [b]Crystallize 4Cs Limited, Oxford, UK

ABSTRACT

Achieving resistance to sedimentation of carbonyl iron powders (CIPs) in ethanol is important to fabricate reliable magnetorheological suspensions. The traditional method to improve the sedimentation stability is to add dispersants, but this approach can suffer from high costs and toxicity of added surfactants. In this study, the surface of CIPs was modified with 3-aminopropyl triethoxysilane (APTES) or tetraethyl orthosilicate (TEOS) to enhance the sedimentation stability of CIP suspensions without using toxic dispersants. After coating APTES or TEOS on the CIP surface, the surface energy of the CIP powders increased, which was attributed to the increased amino or hydroxyl groups on the CIP surface due to APTES or TEOS, respectively. The Gibbs free wetting enthalpy (ΔG) was calculated to evaluate the wettability of the modified CIPs, and APTES@CIPs or TEOS@CIPs had a low ΔG, indicating that both had a high thermodynamic spontaneity of wetting in ethanol. The enhanced wettability due to APTES or TEOS coating resulted in low CIP agglomeration, which resulted in APTES@CIPs or TEOS@CIPs dispersions having smaller average particle sizes than pure CIP dispersions. Therefore, APTES@CIPs or TEOS@CIPs showed more than 2 times slower sedimentation velocity than pure CIPs, resulting in enhanced sedimentation stability.

摘要

实现羰基铁粉（CIPs）在乙醇中的抗沉降性对于制备可靠的磁流变悬浮液至关重要. 提高沉淀稳定性的传统方法是添加分散剂, 但这种方法可能会受到添加表面活性剂的高成本和毒性的影响. 在本研究中, 使用3-氨基丙基三乙氧基硅烷（APTES）或正硅酸乙酯（TEOS）对CIP的表面进行改性, 以提高CIP悬浮液的沉降稳定性, 而不使用有毒分散剂. 在CIP表面涂覆APTES或TEOS后, CIP粉末的表面能增加, 这归因于APTES和TEOS分别导致CIP表面上的氨基或羟基增加. 计算吉布斯自由润湿焓（ΔG）以评估改性CIPs的润湿性, 以及APTES@CIPs或TEOS@CIPsΔG较低, 表明两者在乙醇中润湿具有较高的热力学自发性. APTES或TEOS涂层增强的润湿性导致低CIP团聚, 这导致APTES@CIPs或TEOS@CIPs平均粒径小于纯CIP分散体的分散体. 因此APTES@CIPs或TEOS@CIPs显示出比纯CIPs慢2倍以上的沉降速度, 从而提高了沉降稳定性.

KEYWORDS

Magnetorheological suspension; carbonyl iron powder; sedimentation; surface modification; siloxane; turbiscan

关键词

磁流变悬液; 羰基铁粉; 沉降; 表面改性; 硅氧烷; 涡轮机扫描

Introduction

Smart dispersions that can tune their mechanical properties in response to external stimuli have attracted significant attention in various engineering field applications, such as smart polishing (Alam, Ahmad Khan, and Jha 2018; Zeng and Blunt 2014; Zhang, Kuhlenkötter, and Kneupner 2005), health monitoring (Chong, Kim, and Chon 2013; Shi et al. 2015), or reactive connecting systems (Chen and

CONTACT Byungil Hwang bihwang@cau.ac.kr School of Integrative Engineering,Chung-Ang University, Seoul 06974, Republic of Korea

Supplemental data for this article can be accessed online at https://doi.org/10.1080/15440478.2023.2166648

© 2023 The Author(s). Published with license by Taylor & Francis Group, LLC.
This is an Open Access article distributed under the terms of the Creative Commons Attribution-NonCommercial License (http://creativecommons.org/licenses/by-nc/4.0/), which permits unrestricted non-commercial use, distribution, and reproduction in any medium, provided the original work is properly cited.

Liao 2012; Yoon, Kim, and Choi 2021; Mousavi et al. 2021; Hwang, Han, and Matteini 2022). Magnetorheological (MR) dispersions consisting of magnetic particles and a carrier solvent are the most promising candidate for smart dispersions (Kumar et al. 2019). The degree of arrangement of magnetic particles in a dispersion is controlled by external magnetic fields, which can change the stiffness of MR dispersions in a short time, making them suitable for devices that require performance adjustment in real time (Ahamed, Choi, and Meftahul Ferdaus 2018; Baig and Varma 2013). Several magnetic particles, such as iron, nickel, cobalt, reduced graphene oxide, and MXene, have been used in MR dispersions (Anupama, Kumaran, and Sahoo 2018; Liu et al. 2014; Sun et al. 2022; Tian et al. 2020; Tong, Dong, and Min 2017; Patel and Deheri 2022; Xia et al. 2017). Among them, carbonyl iron powders (CIPs) are the most widely used because of their excellent temperature stability, low eddy current loss, and low cost (Han, Ji Su, and Jin Choi 2020; Małecki et al. 2015; Vicente et al. 2011).

Although CIP-based MR dispersions exhibit excellent magnetic performance in various MR-based devices (Cheng et al. 2022; Miao et al. 2011; Tong et al. 2021), CIPs have difficulties in achieving high resistance to sedimentation in a carrier solvent during storage. The high density CIPs are typically dispersed in low-viscosity solvents such as ethanol or water to form MR dispersions that accelerate the sedimentation by gravitational force (Ilyas, Pendyala, and Marneni 2016). In addition, there is a high probability that CIPs will agglomerate while being mixed with a carrier solvent because of differences in surface characteristics (Bantz et al. 2014; Payrebrune 2022). According to Stoke's law, the sedimentation speed of particles in a solvent is largely governed by the average particle dimensions of the powder in the solvent, as demonstrated by Equation (1):

$$v = \frac{2}{9} g \cdot \frac{r^2 \cdot \left(\rho_p - \rho_l\right)}{\eta}, \tag{1}$$

where v, g, r, ρ_p, ρ_l, and η are the sedimentation velocity, gravitational acceleration, effective powder radius, particle density, liquid density, and liquid viscosity, respectively (Garzanti, Andò, and Vezzoli 2008). CIP agglomeration results in an increase in the effective CIP dimension as a cluster in a solvent; the sedimentation velocity increases accordingly, which degrades the stability of the MR dispersion (Haibin et al. 2018; Jönkkäri, Isakov, and Syrjälä 2014). Therefore, it is crucial to prevent CIP agglomeration in a carrier solvent to obtain high-quality products with MR dispersions.

Tuning the surface of CIPs to be spontaneously wetted in a solvent is one approach to reducing particle agglomeration (Hu et al. 2006; Park, Fei Fang, and Jin Choi 2010). Enhancing the wettability of CIPs in solvents is crucial to achieving high sedimentation stability, as CIPs tend to agglomerate rather than disperse in solvents under low wetting conditions (David et al. 2021; Pulla-Huillca et al. 2021; Song et al. 2019; Zhibin et al. 2020). The Gibbs free energy for wetting (ΔG), which is expressed in Equation (2), is a theoretical indicator for estimating the wettability of particles in a solvent:

$$\Delta G = \gamma_l - 2\left(\sqrt{(\gamma_s^p \cdot \gamma_l^p} + \sqrt{(\gamma_s^D \cdot \gamma_l^D)}\right), \tag{2}$$

where γ_l is the surface tension of the liquid, γ_s^P and γ_l^P are the polar components of the solid surface and liquid, respectively, and γ_s^D and γ_l^D are the dispersive components of the solid surface and liquid, respectively (Bayat et al. 2021; Harikrishnan et al. 2017). A large negative ΔG value indicates that the particles have a high thermodynamic spontaneity for wetting in solvents. According to Equation (2), CIPs that have been modified to have surface polarities that are similar to those of solvents of use have a large negative ΔG; in other words, they have a high thermodynamic spontaneity for wetting, which can enhance their dispersibility in a solvent. Therefore, an appropriate strategy for modifying the surface of CIPs to achieve enhanced wettability is urgently required to enhance the sedimentation stability of CIPs in low-viscosity solvents, such as water, ethanol, and silicon oil.

So far, several studies have been conducted to improve the sedimentation stability and prevent the agglomeration of powder (Ashtiani, Hashemabadi, and Ghaffari 2015; Bombard, Antunes, and

Gouvêa 2009). Adding additive to provide repulsive force in between particles were the generally used strategy to avoid the agglomeration of CIPs in solvents (Kus and Kalin 2019; Liu, Fei Fang, and Jin Choi 2011; Shilko, Grigoriev, and Smolin 2021). However, selecting the appropriate additives for the specific suspension is challenging. In addition, many of additives have issues of high cost and potential toxicity (Yuan et al. 2012). Using a highly viscous solvent is another option to enhance the sedimentation stability, but it is not appropriate for magnetorheological polishing (MRP) that requires a fast response time to the magnetic field (Kumar and Das 2021, 2022; Kumar et al. 2021). To resolve the limitations of the aforementioned technologies, encapsulating CIPs with a functional layer such as siloxane polymer can be considered (Chen et al. 2019; Małecki et al. 2015; Sun et al. 2022). The insulating functional layer prevents the generation of eddy currents that can enhance the absorption performance of electromagnetic waves. Therefore, most of the research on the encapsulation of CIPs with siloxane layer focused on the application of the encapsulated particles to the electromagnetic interference shielding purpose (Chen et al. 2019; Małecki et al. 2015; Sun et al. 2022). By selecting the appropriate functional layer that matches to the functionality of the used solvent, however, the wettability of CIPs can also be enhanced. Theoretically, functional layers with abundant hydroxyl and amino groups such as tetraethyl-orthosilicate (TEOS) and 3-aminopropyl-triethoxysilane (APTES), respectively, will result in spontaneous wetting of CIPs in polar solvents. However, there is a paucity of systematic studies on the change in the sedimentation stability of CIPs by the formation of functional layers.

In this study, CIPs were modified with APTES or TEOS (APTES@CIPs or TEOS@CIPs) to enhance their sedimentation stability in ethanol. APTES- and TEOS-modified CIPs have a hydrophilic nature due to the abundant amino or hydroxyl groups on their surfaces, respectively; thus, the APTES@CIPs and TEOS@CIPs were expected to have better resistance to sedimentation than the pure CIPs due to their enhanced wettability in the hydrophilic ethanol. The sedimentation behavior of the dispersions was systematically evaluated using an in-situ multiple light-scattering system that allowed for the measurement of time-dependent sedimentation profiles. The wettability of the modified CIPs was evaluated by calculating their ΔG, which is an indicator of the thermodynamic spontaneity of particles for wetting in a solvent. The mechanism underlying the change in the sedimentation behavior of the CIP dispersions after modifying the CIP surface with APTES or TEOS was revealed by correlating the sedimentation behavior and wettability test results with the surface microstructural and chemical characteristics analyzed by scanning electron microscopy, Fourier-transform infrared spectroscopy (FTIR), and zeta potential. Additionally, the characterization of the magnetic properties of the modified CIPs revealed the benefits of APTES or TEOS coating for sustaining the magnetic performance of the CIPs. Through this paper, the method for synthesis of siloxane layer on CIP surface was introduced first, and then, the structural analysis of the pure CIPs and the modified CIPs were presented. Next, the sedimentation stability of the different CIP suspension was discussed in correlation with the wettability change by the surface modification of CIPs. Lastly, the effect of siloxane coating on the magnetic performance of CIPs was presented.

Materials and methods

Synthesis of SiO_2 on the CIP surfaces

To create the TEOS@CIPs, 100 g of CIPs (EW grade, average diameter of ~1.5 μm, BASF) was added to 250 mL of 0.5 M hydrochloric acid (HCl; 35%–37%, Daejung Chemical Co. Ltd.) and then sonicated for 30 min to remove the native oxide layer. Thereafter, a permanent magnet was used to make the CIPs settle down at the bottom of a vial. Subsequently, the CIP sediments were separated from the solvent and then sequentially cleaned with ethanol (denatured ethyl alcohol; ~95%) and deionized water (three times each for 15 min). Ethanol (Denatured ethyl alcohol; ~95%; Samchun Chem) and TEOS (≥98.5%; Daejung Chemical Co. Ltd) were mixed at a ratio of 7.6:1 with a total volume of 200 mL, and one drop of HCl, which acted as a catalyst, was added to create an acidic pH environment for

the reaction. The sol-aging process was performed by storing the TEOS/ethanol/HCl mixture for 24 h to allow the reaction to fully develop. Afterward, the surface-treated CIPs were added to the mixture, which was then mechanically stirred at room temperature for 2 h, causing a thick SiO_2 (TEOS) layer to form on the CIP surface. A permanent magnet was used to make the TEOS@CIPs settle down in the vial, and then the solvent was removed from the vial to separate the TEOS@CIPs from the mixture solvent. To remove the organic residue, the TEOS@CIPs were sequentially cleaned with ethanol and deionized water using a bath sonicator for 15 min. Finally, drying was performed in a vacuum oven at 120°C for 12 h to evaporate the remaining ethanol and water on the CIP surface.

To synthesize the APTES@CIPs, 0.4 mL of APTES (≥99%; Sigma-Aldrich) and 3 g of the CIPs that had been treated to remove the native oxide layer were mixed in 120 mL of ethanol using a bath sonicator for 30 min. The CIP/APTES/ethanol mixture was aged for 1 h to form a thick APTES layer. Afterward, the same cleaning procedure used for the TEOS@CIPs was performed. To evaluate the sedimentation behavior, 5 wt% CIPs were dispersed in ethanol using a tip sonicator (60% amplitude of 500 W and 20 kHz) with a tip diameter of 3 mm for 10 min. CIPs can be dispersed up to 60 wt% in ethanol. However, such high volume fraction of CIPs is not suitable for MRP application, where the quick magnetic separation of CIPs from the mixture of CIP and abrasive particles is required. Generally, 1 to 10 wt% is proposed for CIPs in MRP system (Heebo, Thompson, and Hwang 2022; Niranjan and Jha 2014; Viota et al. 2007), and this was why the intermediate 5 wt% was chosen for this study. There is the other method to synthesis siloxane layer using tetramethyl orthosilicate (TMOS). Although the method also can form the siloxane layer well, it uses methanol that is more toxic than ethanol used in our study (Chen et al. 2019; Małecki et al. 2015; Sun et al. 2022). In addition, methanol also has a lower flash point making handling of this solvent more hazardous from flammability considerations. Therefore, the method using TMOS was not considered in this study.

Characterization

The morphology of the CIPs was observed using field-emission SEM (FESEM; S-3400 N, Hitachi). The samples were cut using a focused ion beam (FIB; Helios Nanolab 450 F1) to analyze the cross-sectional images of CIPs. The chemical structure of the APTES or TEOS layer on the CIP surface was analyzed using FTIR. The sedimentation behavior was characterized using Turbiscan AGS (Formulaction, France). The multiple light scattering by Turbiscan is a relative method and not really calibrated to a standard. The contact angle was measured using the Washburn method (Kiesvaara and Yliruusi 1993) and a tensiometer (K100, Kruss, Germany). The particle size of CIPs was measured using PSA (PSA; Microtrac P3000, USA). Before measuring the particle size, calibration was performed to remove the influence of ethanol. The saturation magnetization of the CIPs was measured using a vibrating sample magnetometer (VSM; Lakeshore series-7400, USA) in a magnetic field of 1.5 T at room temperature. The influence of the surrounding environment on the magnetization performance was calibrated for the condition without a sample as well as for the reference Ni powders. Every tests were repeated more than 5 times to have reliable data.

Results and discussion

Figure 1 shows the schematics for the synthesis of APTES and TEOS on the CIP surfaces. The removal of the native oxide layer produced abundant ferric hydroxyl groups on the CIP surface, allowing TEOS or APTES reaction product layers to form on the CIP surface. In ethanol, the ethoxy groups of TEOS were hydrolyzed by CIP hydroxyls to form Si-O bonds (Cvek et al. 2017; Małecki et al. 2015; Zhu et al. 2012). As the hydrolysis process progressed, Si – OH on the CIP surface condensed, thereby forming a continuous SiO_2 layer (siloxane polymer) on the CIP surface. APTES also formed an SiO_2 layer through the hydrolysis process, which caused Si – O bonds to form between APTES and a hydroxyl group on the CIP surface. However, APTES@CIPs had abundant amino ($–NH_2$) groups because the

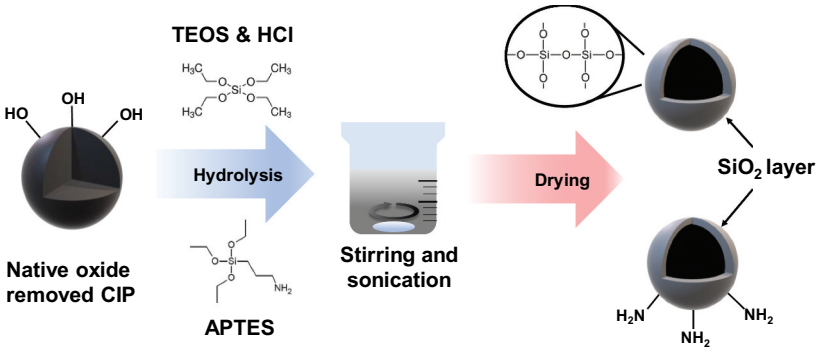


Figure 1. Illustration of modification process of CIP surface with TEOS and APTES.

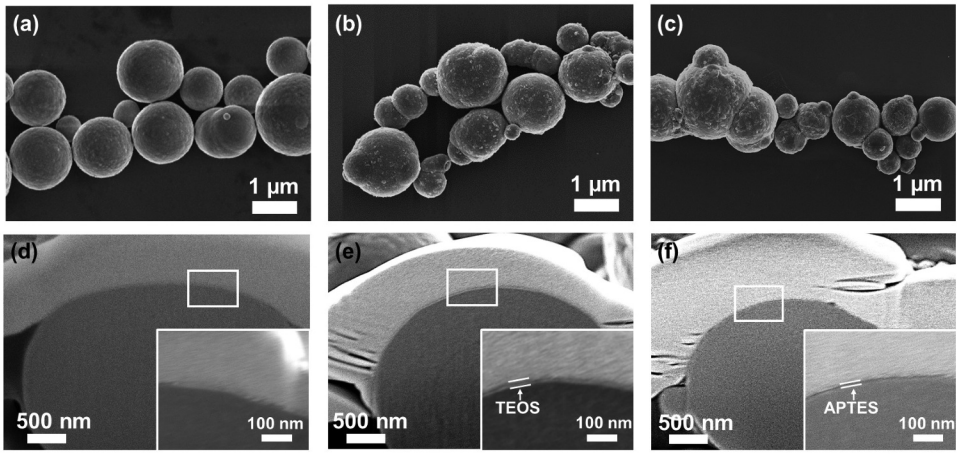


Figure 2. Top view of the SEM images of the (a) CIPs, (b) TEOS@CIPs, and (c) APTES@CIPs. Cross-sectional SEM images of the (f) CIPs, (e) TEOS@CIPs, and (f) APTES@CIPs. The inset shows enlarged images from the white squares in d – f.

amino groups on the surface of the APTES coated surfaces are exposed to the solvent (Li et al. 2015; Zhu et al. 2012).

Figures 2a–c present the top-view SEM images of the pure CIPs, APTES@CIPs, and TEOS@CIPs. The top-view SEM images in Figures 2b and 2c depict the surface modification of the CIPs. Unlike Figures 2a, Figures 2b and 2c depict the surface changes. Figures 2a–c show that the particle sizes are similar to each other. Figures 2d–f show the cross-sectional SEM images of the pure CIPs, APTES@CIPs, and TEOS@CIPs. The APTES@CIP (Figure 2e) and TEOS@CIP (Figure 2F) surfaces had thin layers that were not observed on the pure CIP surface (Figure 2d), indicating that APTES or TEOS formed layers on the CIP surface. APTES and TEOS had thicknesses of ~18.3 ± 4.2 nm and ~37.6 ± 3.7 nm, respectively. With insufficient precursor and reaction time, the modified CIPs showed no significant difference in the sedimentation properties from the un-modified pure CIPs. In addition, in the insufficient condition, the uniformity of the results was very poor; thus, it was rather difficult to show the consistent results. With excess precursor and reaction time, the thickness of siloxane layer increased, but there was no further enhancement of the sedimentation stability once it reached the condition that stated in the section of materials and methods. In addition, the increased thickness of insulating layer on CIPs could degrade the magnetization performance of CIPs. Thus, having the thin but uniform siloxane layer is important to achieve stable MRP with high magnetic performance (Chen et al. 2022; Wang et al. 2015). This was why we chose the single critical conditions where full coverage

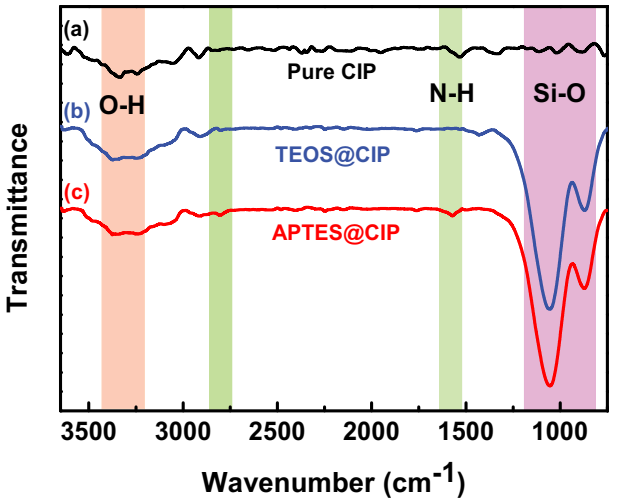


Figure 3. FT-IR spectra of (a) pure CIP, (b) TEOS@CIP and (c) APTES@CIP.

of siloxane layers with the thinnest thickness can be formed on the most of CIPs in a sample. Figure 3 shows the FTIR spectra of the pure CIPs, TEOS@CIPs, and APTES@CIPs. The broad absorption band at 1080 cm^{-1} was observed in both spectra of TEOS@CIPs (Figure 3b), and APTES@CIPs (Figure 3c), which are assigned to the asymmetric stretching of Si-O-Si bonds of TEOS and APTES on the CIP surface. In addition, the peak at 790 cm^{-1} is the symmetric stretch of Si-O bonds, and the peak at 465 cm^{-1} corresponds to bending modes of network and ring opening vibrations of the Si-O bonds of APTES or TEOS. In Figure 3 c, the C-H stretching peaks of APTES on the CIP surface are observed at 2927 and 2855 cm^{-1}. Compared to the pure CIP, the wider absorption band at 3438 and 1600 cm^{-1} are attributed to O-H and N-H vibrations by the amino group of APTES. The cross-sectional SEM images and FTIR analysis results confirmed that the APTES or TEOS layers were well-formed on the CIP surface.

Figure 4 depicts the change in the transmitted (ΔTS) and backscattered (ΔBS) light signals detected in situ for the pure CIPs, APTES@CIPs, and TEOS@CIPs in ethanol after 3 h of settlement. Here, ΔTS

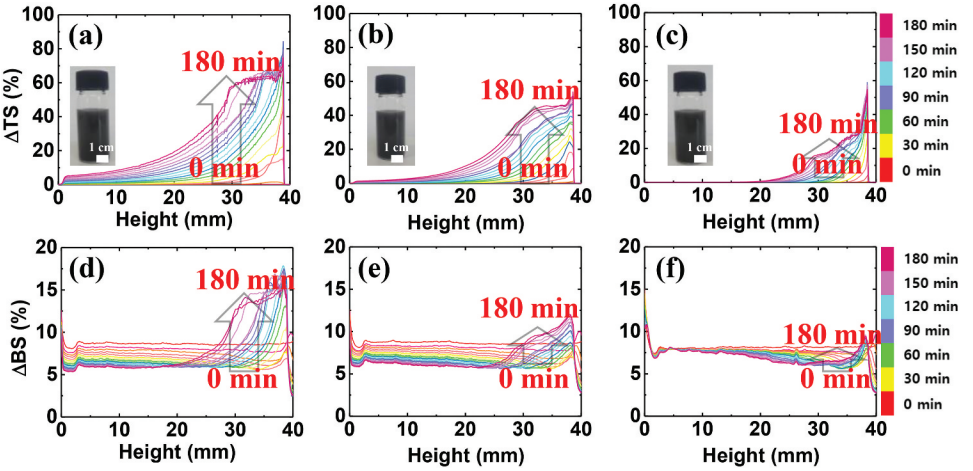


Figure 4. Changes in the transmitted and backscattered values of the suspension containing (a and d) pure CIPs, (b and e) TEOS@CIPs, and (c and f) APTES@CIPS, respectively.

and ΔBS are $|T - T_0|$ and $|BS - BS_0|$, respectively, where T_0 and BS_0 are the measured TS and BS values at the initial scanning, respectively. The measured TS and BS signals in the specific time were presented with the specific colors, which corresponding to the colored time scale shown in the right end of Figure 4. X-axis of Figure 4 indicates the height of sample bottles, where 0 mm is the location of sample bottle and 40 mm is the upmost region of the sample bottle. Since the particles were sediment from the upper part of the sample bottle and the upmost part of the sample bottle was vacant, the rapid change in TS or BS values were started from the upmost part, which were indicated as a sharp peak in Turbiscan profiles (Supporting Information 01). A rapid increase in ΔTS and ΔBS indicates fast sedimentation of particles in a solvent. The pure CIPs exhibited rapid sedimentation, with a 10% increase in ΔTS values throughout settling at the bottom region. After coating with TEOS or APTES, the sedimentation speed decreased, with TEOS@CIPs and APTES@CIPs exhibiting a 5% increase and a 1% increase in ΔTS values, respectively. The ΔTS values of the pure CIPs exhibited similar trends to those of TEOS@CIPs and APTES@CIPs; however, the TEOS@CIPs and APTES@CIPs exhibited a much smaller increase in ΔTS values during the test periods.

The sedimentation behavior can be intuitively compared by calculating the Turbiscan stability index (TSI) using equation. (Ramirez et al.):

$$TSI(t) = 1/N_h + \sum_{t_i=0}^{t_{max}} \sum_{z_i=z_{min}}^{z_{max}} |BST(t_i, z_i) - BST(t_{i-1}, z_i)|, \text{(Ramirez et al.)}$$

where t_{max}, z_{min}, z_{max}, N_h, and BST (backscattering and transmission) are the scanning time for measuring the TS or BS signals, the bottom height limit, the top height limit, the number of scanned positions in the measured area $((z_{max} - z_{min})/\Delta h)$, and the signal considered for the TSI calculation, respectively (Heebo, Thompson, and Hwang 2022; Luo et al. 2017). TSI values provide the average values of the sedimentation progress in a specific position and time (Pan et al. 2021). Samples that exhibit fast sedimentation have high TSI values. Figure 5 depicts the calculated TSI values of the dispersions containing the pure CIPs, APTES@CIPs, and TEOS@CIPs as functions of the settlement time. The pure CIPs, TEOS@CIPs, and APTES@CIPs had TSI values of ~34, ~25, and ~12 at 180 min, respectively. The TSI values of APTES@CIPs and TEOS@CIPs were about 3 and 2 times lower than those of pure CIPs, respectively, indicating that the sedimentation stability noticeably improved after APTES or TEOS coating. Additionally, APTES was discovered to be more effective in enhancing sedimentation stability than TEOS. The pendant amino groups can become protonated to develop

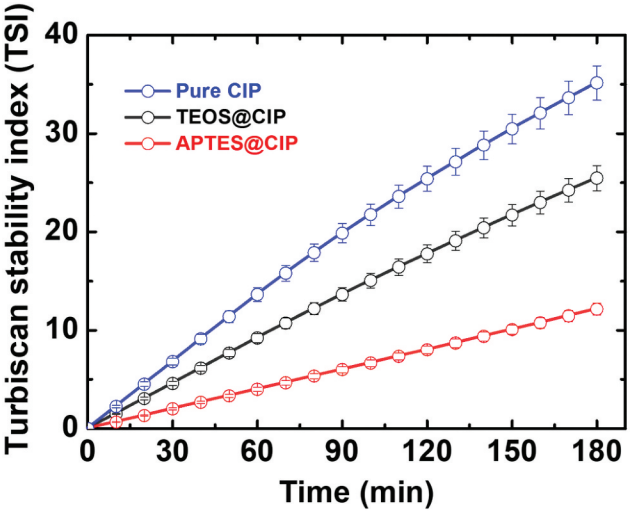


Figure 5. Turbiscan stability index values of the suspensions containing the various CIP types as functions of time.

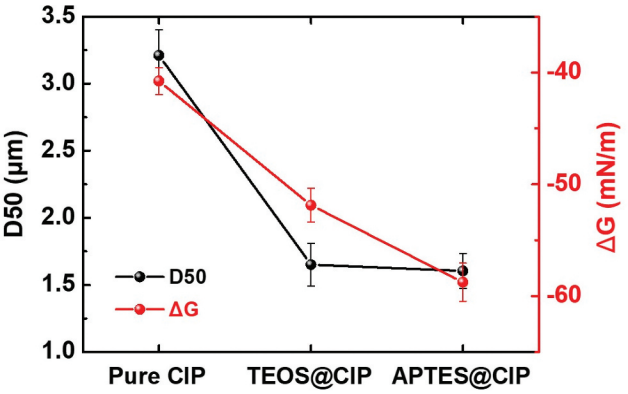


Figure 6. D50 and ΔG values of the various CIP types based on the different coatings.

a positive (cationic) surface charge on CIP, which might lead to a colloidal electrostatic stabilization mechanism in ethanol solvent (Ginés et al. 2017).

After modifying the CIP surface, the APTES@CIPs and TEOS@CIPs were much less agglomerated so exhibit smaller average particle sizes for the agglomerates than untreated CIP. According to Stoke's law (Equation (1)), the smaller particle size results in the slower sedimentation velocity. This is because there were no different conditions in the dispersion other than the change in particle size, which is caused by particle agglomeration in solvents. The average particle sizes of the agglomerated pure CIPs, APTES@CIPs, and TEOS@CIPs were measured using a PSA. The D50 values of APTES@CIPs and TEOS@CIPs were 1.60 ± 0.13 and 1.65 ± 0.16 μm, respectively, which were smaller than that of the pure CIPs (3.21 ± 0.19 μm; Figure 6 and Supporting information 02). The small particle sizes indicate that APTES@CIPs and TEOS@CIPs exhibited reduced agglomeration. The reduced agglomeration can be attributed to the enhanced wettability of the CIPs after surface modification with APTES or TEOS. The ΔG values for the pure CIPs, APTES@CIPs, and TEOS@CIPs were calculated to evaluate the wettability. Table 1 lists the surface characteristics used for the ΔG calculation. The contact angle of the CIPs was measured using the Washburn method, and the surface energy was calculated using the Owens, Wendt, Rabel, and Kaelble (OWRK) model (Cappelletti et al. 2013). The APTES@CIPs and TEOS@CIPs had lower ΔG values than the pure CIPs. Thus, the APTES@CIPs and TEOS@CIPs were expected to have enhanced thermodynamic spontaneity for wetting in ethanol. APTES and TEOS have a hydrophilic nature due to the abundant amino or hydroxyl groups on their surfaces, respectively; thus, the surface energy of the CIPs increased after APTES or TEOS coating (Table 1). The amino groups in APTES or the hydroxyl groups in TEOS also resulted in high absolute zeta potential values, with the APTES@CIPs and TEOS@CIPs having values of 78.2 and 57.1 mV, respectively, whereas the pure CIPs displayed −55.4 mV. Accordingly, the fraction of polar components of the surface energy, i.e. polarity, increased and approached the ethanol values. According to Equation (2), a small polarity mismatch between the powder and solvent results in large negative ΔG values. Therefore, the wetting of the APTES@CIPs or TEOS@CIPs with smaller (i.e. larger negative) ΔG values in ethanol was thermodynamically more favorable than that of the pure CIPs, which contributed to the reduced

Table 1. Surface characteristics of the pure CIPs, APTES@CIPs, and TEOS@CIPs.

	Contact angle (°)					
	Polar (Water)	Nonpolar (Diiodomethane)	Surface tension (mJ/m^2)	Dispersive component (mJ/m^2)	Polar component (mJ/m^2)	ΔG with ethanol (mN/m)
CIP	~83	~25	48.1	46.1	2.0	−40.8
TEOS@CIP	~52	~16	62.0	47.5	14.5	−51.9
APTES@CIP	~25	~15	76.0	49.1	26.9	−58.8
Ethanol			22.1	17.5	4.6	

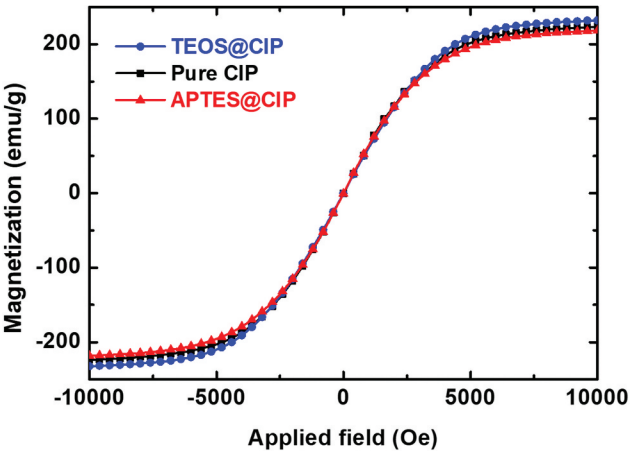


Figure 7. Hysteresis loops of the various CIP types based on the different coatings at room temperature.

agglomeration tendency. Additionally, the APTES@CIPs had smaller ΔG values than the TEOS@CIPs, which is consistent with the sedimentation stability trend observed during the Turbiscan tests.

To confirm the effect of APTES or TEOS coating on the magnetic properties of the CIPs, the hysteresis loops of the saturation magnetization (Ginés et al.) vs. applied magnetic field for the pure CIPs, APTES@CIPs, and TEOS@CIPs were measured using a VSM at room temperature, as shown in Figure 7. Overall, all the samples exhibited the behavior of soft magnetic materials, which have magnetic properties, such as high magnetic induction, high permeability, and low magnetic limitations. Additionally, the pure CIPs, APTES@CIPs, and TEOS@CIPs had similar Ms values, which were 223.83, 218.15, and 231.96 emu/g, respectively. These results confirm that the APTES or TEOS coating had no degradable effect on the magnetic properties of the CIPs.

Conclusion

In this study, the effect of APTES or TEOS coating on the sedimentation behavior of CIP suspensions in ethanol solvent was explored using an in situ multiple light-scattering method. APTES or TEOS was coated on the CIPs to form a stable siloxane polymer SiO_2 layer on the CIP surfaces, which was confirmed by the cross-sectional SEM images and FTIR analysis. The sedimentation behavior of the samples was characterized with in situ multiple light-scanning method using a Turbiscan. The results revealed that the TEOS@CIPs and APTES@CIPs exhibited better sedimentation stability than the pure CIPs. According to Stoke's law, the enhanced sedimentation stability was attributed to the smaller effective diameters of the TEOS@CIPs and APTES@CIPs agglomerates than those of the pure CIPs. The PSA analysis revealed that the D50 values of TEOS@CIPs or APTES@CIPs agglomerates were about two times smaller than that of the pure CIPs. APTES or TEOS coating provided abundant amino or hydroxyl groups on the CIP surface, respectively, which enhanced wettability in ethanol due to the high thermodynamic spontaneity of wetting, which was caused by a decrease in the surface polarity mismatch. Low wettability accelerated the agglomeration of the CIPs in a solvent, which increased the effective diameter of the CIP clusters and accelerated their sedimentation in the solvent. The VSM analysis further revealed that the APTES or TEOS coating did not significantly degrade the magnetic properties of the CIPs. Thus, APTES or TEOS coating is an effective strategy for enhancing the sedimentation stability of CIPs in magnetorheological suspensions while sustaining their excellent magnetic properties. In addition, the corrosion of CIPs in water solvent will have serious effects on the sedimentation stability and magnetic performance of MRP system. The APTES or TEOS coating might delay the corrosion velocity of CIPs by blocking the CIP surfaces from the corrosive

environment. However, the corrosion tests were beyond the current capability of our laboratory, but it will be definitely studied as the next step of this development work in the future.

Highlights

- CIPs were encapsulated with hydrophilic siloxane polymer coatings, such as APTES or TEOS.
- The APTES or TEOS coating enhanced the wettability of CIPs in ethanol due to the high thermodynamic spontaneity of wetting.
- Agglomeration of the CIPs was prevented by the APTES or TEOS coating, thereby improving the sedimentation stability.
- The APTES or TEOS coating showed no significant change in magnetic property of CIPs.

Acknowledgement

This work was supported by the National Research Foundation of Korea (NRF) (Nos. 2022R1F1A1063696 and 2021K1A3A1A74096164).

Disclosure statement

No potential conflict of interest was reported by the authors.

Funding

The work was supported by the National Research Foundation of Korea [2021K1A3A1A74096164]; National Research Foundation of Korea [2022R1F1A1063696].

References

Ahamed, R., S. B. Choi, and M. Meftahul Ferdaus. 2018. A state of art on magneto-rheological materials and their potential applications. *Journal of Intelligent Material Systems and Structures* 29 (10):2051–95. doi:10.1177/1045389x18754350.

Alam, Z., D. Ahmad Khan, and S. Jha. 2018. MR fluid-based novel finishing process for nonplanar copper mirrors. *International Journal of Advanced Manufacturing Technology* 101 (1–4):995–1006. doi:10.1007/s00170-018-2998-2.

Anupama, A. V., V. Kumaran, and B. Sahoo. 2018. Application of monodisperse Fe3O4 submicrospheres in magnetorheological fluids. *Journal of Industrial and Engineering Chemistry* 67:347–57. doi:10.1016/j.jiec.2018.07.006.

Ashtiani, M., S. H. Hashemabadi, and A. Ghaffari. 2015. A review on the magnetorheological fluid preparation and stabilization. *Journal of Magnetism and Magnetic Materials* 374:716–30. doi:10.1016/j.jmmm.2014.09.020.

Baig, R. B., and R. S. Varma. 2013. Magnetically retrievable catalysts for organic synthesis. *Chemical Communications (Cambridge, England)* 49 (8):752–70. doi:10.1039/c2cc35663e.

Bantz, C., O. Koshkina, T. Lang, H. J. Galla, C. J. Kirkpatrick, R. H. Stauber, and M. Maskos. 2014. The surface properties of nanoparticles determine the agglomeration state and the size of the particles under physiological conditions. *Beilstein Journal of Nanotechnology* 5:1774–86. doi:10.3762/bjnano.5.188.

Bayat, A., M. Ebrahimi, S. R. Ardekani, E. S. Iranizad, and A. Z. Moshfegh. 2021. Extended Gibbs Free Energy and Laplace Pressure of Ordered Hexagonal Close-Packed Spherical Particles: A Wettability Study. *Langmuir* 37 (28):8382–92. doi:10.1021/acs.langmuir.1c00343.

Bombard, A. J. F., L. S. Antunes, and D. Gouvêa. 2009. "Redispersibility in magnetorheological fluids: Surface interactions between iron powder and wetting additives." *Journal of Physics: Conference Series* 149. doi: 10.1088/1742-6596/149/1/012038.

Cappelletti, G., S. Ardizzone, D. Meroni, G. Soliveri, M. Ceotto, C. Biaggi, M. Benaglia, and L. Raimondi. 2013. Wettability of bare and fluorinated silanes: A combined approach based on surface free energy evaluations and dipole moment calculations. *Journal of Colloid and Interface Science* 389 (1):284–91. doi:10.1016/j.jcis.2012.09.008.

Cheng, H., T. Lim, S. Kim, and W. Jung. 2022. Sound insulation effect of magnetorheological fluid as a function of magnetic field strength and direction. *Materials Research Letters* 10 (5):310–17. doi:10.1080/21663831.2022.2050431.

Chen, C., and W. H. Liao. 2012. A self-sensing magnetorheological damper with power generation. *Smart Materials and Structures* 21 (2). doi: 10.1088/0964-1726/21/2/025014.

Chen, Q., L. Liya, Z. Wang, G. Yicheng, C. Zhou, and Y. Jianhong. 2019. Synthesis and enhanced microwave absorption performance of CIP@ SiO2@mn0.6zn0.4fe2o4 ferrite composites. *Journal of Alloys and Compounds* 779:720–27. doi:10.1016/j.jallcom.2018.11.112.

Chen, Z., J. Pan, Q. Yan, Z. Huang, F. Zhang, and S. Chen. 2022. Study on the rheological and polishing properties of electromagnetic two-phase composite particles with abrasive characteristics. *Smart Materials and Structures* 31 (4). doi: 10.1088/1361-665X/ac5478.

Chong, J. W., Y. Kim, and K. H. Chon. 2013. Nonlinear multiclass support vector machine–based health monitoring system for buildings employing magnetorheological dampers. *Journal of Intelligent Material Systems and Structures* 25 (12):1456–68. doi:10.1177/1045389x13507343.

Cvek, M., R. Moucka, M. Sedlacik, and V. Pavlinek. 2017. Electromagnetic, magnetorheological and stability properties of polysiloxane elastomers based on silane–modified carbonyl iron particles with enhanced wettability. *Smart Materials and Structures* 26 (10). doi: 10.1088/1361-665X/aa85c5.

David, F., R. Sharma, S. I. Takeda, T. Cosgrove, and S. W. Prescott. 2021. Fast NMR relaxation, powder wettability and Hansen solubility parameter analyses applied to particle dispersibility. *Powder Technology* 377:545–52. doi:10.1016/j.powtec.2020.09.002.

De Payrebrune, K. M. 2022. Relation of kinematics and contact forces in three-body systems with a limited number of particles. *Facta Universitatis, Series: Mechanical Engineering* 20 (1):95–108. doi:10.22190/FUME210310035P.

Garzanti, E., S. Andò, and G. Vezzoli. 2008. Settling equivalence of detrital minerals and grain-size dependence of sediment composition. *Earth and Planetary Science Letters* 273 (1–2):138–51. doi:10.1016/j.epsl.2008.06.020.

Ginés, L., S. Mandal, A. I. Ahmed Ashek-I-Ahmed, C. L. Cheng, M. Sow, and O. A. Williams. 2017. Positive zeta potential of nanodiamonds. *Nanoscale* 9 (34):12549–55. doi:10.1039/c7nr03200e.

Haibin, C., M. Wang, C. Liu, and N. M. Wereley. 2018. Improving sedimentation stability of magnetorheological fluids using an organic molecular particle coating. *Smart Materials and Structures* 27 (7). doi: 10.1088/1361-665X/aabf13.

Han, W. J., A. Ji Su, and H. Jin Choi. 2020. Enhanced magnetorheological characteristics of hollow magnetite nanoparticle-carbonyl iron microsphere suspension. *Smart Materials and Structures* 29 (5). doi: 10.1088/1361-665X/ab7f43.

Harikrishnan, A. R., S. K. Das, P. K. Agnihotri, and P. Dhar. 2017. Particle and surfactant interactions effected polar and dispersive components of interfacial energy in nanocolloids. *Journal of Applied Physics* 122 (5). doi: 10.1063/1.4997123.

Heebo, H., R. Thompson, and B. Hwang. 2022. Iron oxide layer effects on the sedimentation behavior of carbonyl iron powder suspension. *Colloid and Interface Science Communications* 50. doi:10.1016/j.colcom.2022.100670.

Heebo, H., R. Thompson, P. Matteini, S. Jo Yoo, and B. Hwang. 2022. Effect of surface change by vacuum drying on the sedimentation stability of iron nanoparticles in volatile organic solvents. *Colloid and Interface Science Communications* 48. doi:10.1016/j.colcom.2022.100625.

Hu, B., A. Fuchs, S. Huseyin, F. Gordaninejad, and C. Evrensel. 2006. Atom transfer radical polymerized MR fluids. *Polymer* 47 (22):7653–63. doi:10.1016/j.polymer.2006.08.069.

Hwang, B., Y. Han, and P. Matteini. 2022. Bending fatigue behavior of ag nanowire/cu thin-film hybrid interconnects for wearable electronics. *Facta Universitatis, Series: Mechanical Engineering* 20 (3):553–60. doi:10.22190/FUME220730040H.

Ilyas, S. U., R. Pendyala, and N. Marneni. 2016. Stability and Agglomeration of Alumina Nanoparticles in Ethanol-Water Mixtures. *Procedia Engineering* 148:290–97. doi:10.1016/j.proeng.2016.06.616.

Jönkkäri, I., M. Isakov, and S. Syrjälä. 2014. Sedimentation stability and rheological properties of ionic liquid–based bidisperse magnetorheological fluids. *Journal of Intelligent Material Systems and Structures* 26 (16):2256–65. doi:10.1177/1045389x14551436.

Kiesvaara, J., and J. Yliruusi. 1993. The use of the Washburn method in determining the contact angles of lactose powder. *International Journal of Pharmaceutics* 92 (1):81–88. doi:10.1016/0378-5173(93)90266-I.

Kumar, M., A. Alok, V. Kumar, and M. Das. 2021. Advanced abrasive-based nano-finishing processes: Challenges, principles and recent applications. *Materials and Manufacturing Processes* 37 (4):372–92. doi:10.1080/10426914.2021.2001509.

Kumar, M., and M. Das. 2021. Improvement in Surface Characteristics of SS316L tiny gear profiles by magnetorheological-polishing fluid using flow restrictor. *Transactions of the Indian Institute of Metals* 74 (12):3035–44. doi:10.1007/s12666-021-02339-x.

Kumar, M., and M. Das. 2022. Performance Evaluation of Rotational-Magnetorheological Glass–Ceramic Polishing (R-MRGP) Process Setups. *Arabian Journal for Science and Engineering* 47 (12):15269–84. doi:10.1007/s13369-021-06504-8.

Kumar, J. S., P. Sam Paul, G. Raghunathan, and D. George Alex. 2019. A review of challenges and solutions in the preparation and use of magnetorheological fluids. *International Journal of Mechanical and Materials Engineering* 14 (1). doi: 10.1186/s40712-019-0109-2.

Kus, M., and M. Kalin. 2019. Influence of additives and their molecular structure on the static and dynamic wetting of oil on steel at room temperature. *Applied Surface Science* 490:420–29. doi:10.1016/j.apsusc.2019.06.111.

Li, J., W. J. Feng, J. S. Wang, X. Zhao, W. Q. Zheng, and H. Yang. 2015. Impact of silica-coating on the microwave absorption properties of carbonyl iron powder. *Journal of Magnetism and Magnetic Materials* 393:82–87. doi:10.1016/j.jmmm.2015.05.049.

Liu, Y. D., F. Fei Fang, and H. Jin Choi. 2011. Core–shell-structured silica-coated magnetic carbonyl iron microbead and its magnetorheology with anti-acidic characteristics. *Colloid and Polymer Science* 289 (11):1295–98. doi:10.1007/s00396-011-2452-6.

Liu, X., L. Wang, H. Lu, D. Wang, Q. Chen, and Z. Wang. 2014. A study of the effect of nanometer Fe_3O_4 addition on the properties of silicone oil-based magnetorheological fluids. *Materials and Manufacturing Processes* 30 (2):204–09. doi:10.1080/10426914.2014.941875.

Luo, M., Q. Xuejiao, T. Ren, Y. Huang, A. A. Keller, H. Wang, W. Boran, H. Jin, and L. Fengting. 2017. Heteroaggregation of CeO2 and TiO2 engineered nanoparticles in the aqueous phase: Application of turbiscan stability index and fluorescence excitation-emission matrix (EEM) spectra. *Colloids and Surfaces A: Physicochemical and Engineering Aspects* 533:9–19. doi:10.1016/j.colsurfa.2017.08.014.

Małecki, P., K. Kolman, J. Pigłowski, J. Kaleta, and J. Krzak. 2015. Sol–gel method as a way of carbonyl iron powder surface modification for interaction improvement. *Journal of Solid State Chemistry* 226:224–30. doi:10.1016/j.jssc.2015.03.002.

Miao, C., R. Shen, M. Wang, S. N. Shafrir, H. Yang, and S. D. Jacobs. 2011. Rheology of Aqueous Magnetorheological Fluid Using Dual Oxide-Coated Carbonyl Iron Particles. *Journal of the American Ceramic Society* 94 (8):2386–92. doi:10.1111/j.1551-2916.2011.04423.x.

Mousavi, S. M., M. N. Rostami, M. Yousefi, and S. Dinarvand. 2021. Dual solutions for MHD flow of a water-based TiO2-Cu hybrid nanofluid over a continuously moving thin needle in presence of thermal radiation. *Reports in Mechanical Engineering* 2 (1):31–40. doi:10.31181/rme200102031m.

Niranjan, M. S., and S. Jha. 2014. Flow Behaviour of Bidisperse MR Polishing Fluid and Ball End MR Finishing. *Procedia Materials Science* 6:798–804. doi:10.1016/j.mspro.2014.07.096.

Pan, Y., X. Yangyang, L. Zhu, X. Liu, G. Zhao, S. Wang, L. Yang, M. Tao, and H. Liu. 2021. Stability and rheological properties of water-in-oil (W/O) emulsions prepared with a soyasaponin-PGPR system. *Future Foods* 4. doi:10.1016/j.fufo.2021.100096.

Park, B. J., F. Fei Fang, and H. Jin Choi. 2010. Magnetorheology: Materials and application. *Soft Matter* 6 (21). doi: 10.1039/c0sm00014k.

Patel, J., and G. M. Deheri. 2022. Influence of viscosity variation on ferrofluid based long bearing. *Reports in Mechanical Engineering* 3 (1):37–45. doi:10.31181/rme200103037j.

Pulla-Huillca, P. V., A. Gomes, A. Mônica Quinta Barbosa Bittante, R. V. Lourenço, and P. J. D. A. Sobral. 2021. Wettability of gelatin-based films: The effects of hydrophilic or hydrophobic plasticizers and nanoparticle loads. *Journal of Food Engineering* 297. doi:10.1016/j.jfoodeng.2021.110480.

Ramirez, J., A. D. Urbina, A. T. Kleinschmidt, S. J. E. M Finn 3rd, G. L. Esparza, and D. J. Lipomi. 2020. Exploring the limits of sensitivity for strain gauges of graphene and hexagonal boron nitride decorated with metallic nanoislands. *Nanoscale* 12 (20):11209–21. doi:10.1039/d0nr02270e.

Shilko, E. V., A. S. Grigoriev, and A. Y. Smolin. 2021. A discrete element formalism for modelling wear particle formation in contact between sliding metals. *Facta Universitatis, Series: Mechanical Engineering* 19 (1):7–22. doi:10.22190/FUME201221012S.

Shi, D., M. E. Sadat, A. W. Dunn, and D. B. Mast. 2015. Photo-fluorescent and magnetic properties of iron oxide nanoparticles for biomedical applications. *Nanoscale* 7 (18):8209–32. doi:10.1039/c5nr01538c.

Song, K., J. Lee, S. O. Choi, and J. Kim. 2019. Interaction of Surface Energy Components between Solid and Liquid on Wettability, and Its Application to Textile Anti-Wetting Finish. *Polymers (Basel)* 11 (3). doi: 10.3390/polym11030498.

Sun, Y., Y. Wang, H. Deng, M. Sang, and X. Gong. 2022. Effect of MXene nanosheets attached to carbonyl iron microspheres on the performance and stability of magnetorheological fluid. *Journal of Industrial and Engineering Chemistry* 114:508–17. doi:10.1016/j.jiec.2022.07.040.

Tian, F., J. F. Zhou, C. L. Shao, W. Hong-Bo, and L. Hao. 2020. Effective recovery of oil slick using the prepared high hydrophobic and oleophilic Fe3O4 magnetorheological fluid. *Colloids and Surfaces A: Physicochemical and Engineering Aspects* 591. doi:10.1016/j.colsurfa.2020.124531.

Tong, Y., X. Dong, and Q. Min. 2017. High performance magnetorheological fluids with flower-like cobalt particles. *Smart Materials and Structures* 26 (2). doi: 10.1088/1361-665X/aa57cc.

Tong, Y., L. Xiaoguang, P. Zhao, X. Dong, W. Zhanjun, and Q. Min. 2021. Improved Magnetorheological Properties by Using Ionic Liquid as Carrier Liquid of Magnetorheological Fluids. *Frontiers in Materials* 8. doi:10.3389/fmats.2021.659998.

Vicente, D., D. Juan, J. Klingenberg, and R. Hidalgo-Alvarez. 2011. Magnetorheological fluids: A review. *Soft Matter* 7 (8). doi: 10.1039/c0sm01221a.

Viota, J. L., J. D. G. Durán, F. González-Caballero, and A. V. Delgado. 2007. Magnetic properties of extremely bimodal magnetite suspensions. *Journal of Magnetism and Magnetic Materials* 314 (2):80–86. doi:10.1016/j.jmmm.2007.02.002.

Wang, H., D. Zhu, W. Zhou, and F. Luo. 2015. Electromagnetic property of SiO2-coated carbonyl iron/polyimide composites as heat resistant microwave absorbing materials. *Journal of Magnetism and Magnetic Materials* 375:111–16. doi:10.1016/j.jmmm.2014.09.061.

Xia, Z., W. Xiaoxiao, G. Peng, L. Wang, L. Weihua, and W. Wen. 2017. A novel nickel nanowire based magnetorheological material. *Smart Materials and Structures* 26 (5). doi: 10.1088/1361-665X/aa5bd0.

Yoon, D. S., G. W. Kim, and S. B. Choi. 2021. Response time of magnetorheological dampers to current inputs in a semi-active suspension system: Modeling, control and sensitivity analysis. *Mechanical Systems and Signal Processing* 146. doi:10.1016/j.ymssp.2020.106999.

Yuan, Y., D. Rende, C. L. Altan, S. Bucak, R. Ozisik, and D. A. Borca-Tasciuc. 2012. Effect of surface modification on magnetization of iron oxide nanoparticle colloids. *Langmuir* 28 (36):13051–59. doi:10.1021/la3022479.

Zeng, S., and L. Blunt. 2014. Experimental investigation and analytical modelling of the effects of process parameters on material removal rate for bonnet polishing of cobalt chrome alloy. *Precision Engineering* 38 (2):348–55. doi:10.1016/j.precisioneng.2013.11.005.

Zhang, X., B. Kuhlenkötter, and K. Kneupner. 2005. An efficient method for solving the Signorini problem in the simulation of free-form surfaces produced by belt grinding. *International Journal of Machine Tools & Manufacture* 45 (6):641–48. doi:10.1016/j.ijmachtools.2004.10.006.

Zhibin, S., L. Yiping, W. Ying, L. Jiao, and J. Dongsheng. 2020. Study on sedimentation stability of magnetorheological fluids based on different lubricant formulations. *Materials Research Express* 7 (8):085702. doi:10.1088/2053-1591/abb055.

Zhu, J., S. Wei, I. Y. Lee, S. Park, J. Willis, N. Haldolaarachchige, D. P. Young, Z. Luo, and Z. Guo. 2012. Silica stabilized iron particles toward anti-corrosion magnetic polyurethane nanocomposites. *RSC Advances* 2 (3):1136–43. doi:10.1039/c1ra00758k.